

# Multiterminal Ballistic Josephson Effect in Monocrystalline Gold

K.B. Polevoy,<sup>1,2</sup> G.A. Bobkov,<sup>1</sup> D.S. Kalashnikov,<sup>1</sup> A.G. Shishkin,<sup>1</sup> I.V. Trofimov,<sup>3,1</sup>  
A.M. Bobkov,<sup>1</sup> M.A. Tarkhov,<sup>3,1</sup> I.V. Bobkova,<sup>1,4</sup> and V. S. Stolyarov<sup>1,2</sup>

<sup>1</sup>*Moscow Institute of Physics and Technology, Dolgoprudny, 141700 Moscow region, Russia*

<sup>2</sup>*All-Russian Research Institute of Automatics n.a. N.L. Dukhov (VNIIA), 127030, Moscow, Russia*

<sup>3</sup>*Institute of Nanotechnology of Microelectronics of RAS, Moscow, Russia*

<sup>4</sup>*HSE University, 101000 Moscow, Russia*

We report on the realization of a planar, quasi-ballistic Josephson junction array using a Au micron-sized single-crystal. The system exhibits a nonlocal, multiterminal Josephson effect, where the supercurrent between any two superconducting leads is governed by the phase coherence across the entire crystal. Key evidence includes a non-monotonic dependence of the critical current on junction length and magnetic interference patterns with periods corresponding to the shared normal-metal area. Nonlocal transport measurements further confirm that the supercurrent between two electrodes depends on the phase configuration of all the others. Our results, supported by a developed theoretical model, establish a platform for exploring complex superconducting phenomena in multiterminal ballistic systems.

*Introduction.*—The Josephson effect continues to inspire fundamental research and technological applications since its discovery in 1962 [1]. Planar Josephson junction technology offers a promising route to miniaturize weak-link regions to 100–200 nm while maintaining high critical currents  $I_c$  and characteristic voltages  $V_c = I_c R_N$ . Typically, such Josephson junctions comprise a normal metal (N) nanowire or film with two superconductor electrodes (S) deposited on top [2–20], forming complex SN/N/SN Josephson junctions (JJs) in bridge geometry. Most experimental and theoretical studies [21–26] address the diffusive regime, where the mean free path  $l$  is less than the superconducting coherence length  $\xi_N$ .

Planar ballistic JJs, enabling Josephson coupling over micron-scale distances, provide a unique platform for studying proximity-induced superconductivity in the ballistic regime. Up to now, the ballistic JJs have been mainly implemented and studied experimentally in heterostructures of graphene [27–32]. Moreover, in more complex S/N/S structures, where a normal metal is proximitized by several superconducting electrodes, novel effects come into play. In particular, the energy spectrum of a multi-terminal Josephson device can emulate a band structure supporting Weyl points, where the superconducting phases play the role of quasi-momenta [33–35]. Thus, multi-terminal Josephson junctions are expected to be a platform for designing and studying the topological matter of arbitrary dimensions. Several groups have already implemented mesoscopic JJs with three or four terminals in diffusive metallic junctions [36–38], hybrid semiconductor-superconductor heterostructures [39–42], and topological materials [43]. Ballistic JJs are particularly attractive for multiterminal systems, as they facilitate efficient coupling between leads separated by several microns, as demonstrated in graphene [44–46].

In this Letter, we present a combined experimental and theoretical study of planar, quasi-ballistic multi-terminal JJs comprising Al superconducting leads on a gold single

crystal. We investigate supercurrent flow as a function of temperature and magnetic field and develop a microscopic quasiclassical theory for quasiballistic transport in multi-terminal planar S/N/S structures. The theory agrees quantitatively with experiments, confirming the realization of a planar multi-terminal Josephson system in the quasi-ballistic regime.

*Sample fabrication and characterization.*—We fabricate ballistic Josephson junctions by depositing aluminum ( $d_{\text{Al}} = 175$  nm) through an electron-beam lithography mask onto a mechanically transferred monocrystalline Au flake ( $d_{\text{Au}} = 80$  nm, lateral size 14  $\mu\text{m}$ ) on a  $\text{SiO}_2/\text{Si}$  substrate. The monocrystalline Au flakes were synthesized using a modified Brust-Schiffrin method followed by thermolysis, as described in Ref. [47–49]. The Au flake was transferred onto the substrate using an all-dry viscoelastic stamping technique with a polyvinyl chloride/polydimethylsiloxane (PVC/PDMS) stamp [50]. Figure 1(a) shows a false-colored SEM image of the device, with eight Al electrodes (labeled  $A_1$ – $A_4$  and  $B_1$ – $B_4$ ) contacting the Au crystal for standard four-probe dc measurements. The inset schematically shows the additional four-probe dc measurement configuration. Transport measurements are performed in a dilution refrigerator using filtered dc lines. From resistivity measurements,  $\rho(300\text{ K}) = 20.70\text{ n}\Omega \cdot \text{m}$  and  $\rho(4\text{ K}) = 1.35\text{ n}\Omega \cdot \text{m}$ , we extract a low-temperature electron mean free path,  $l = 680$  nm. The junction lengths are  $L_1^{JJ} = 94$  nm,  $L_2^{JJ} = 258$  nm,  $L_3^{JJ} = 614$  nm, and  $L_4^{JJ} = 1008$  nm. Each lead has a length of  $\sim 7\text{ }\mu\text{m}$  and a width  $w = 570$  nm, with an inter-lead spacing of  $W = 1\text{ }\mu\text{m}$ .

*Zero-field critical currents.*—Figure 1(b) displays the temperature dependence of the critical current  $I_c$  for  $A_i$ – $B_i$  junctions ( $i = 1$ –4). Strikingly,  $I_c$  depends non-monotonically on interlayer length  $L_i^{JJ}$ : the critical currents of the two middle JJs  $I_c^{A_2-B_2}(T = 200\text{ mK}) \approx I_c^{A_3-B_3}(T = 200\text{ mK}) = I_c^m$  are very close to each other and exceed the currents of the two outer JJs  $I_c^{A_1-B_1}(T =$

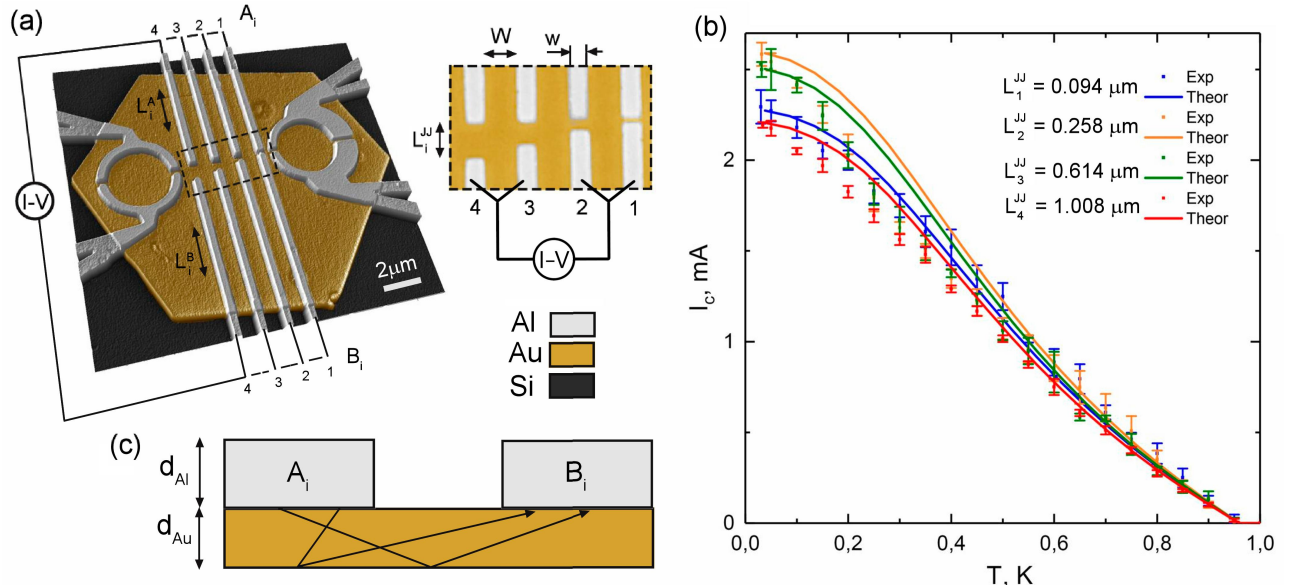


FIG. 1. (a) False-colored SEM image of the Josephson junction array with Al electrodes (labeled  $A_1$ – $A_4$ ,  $B_1$ – $B_4$ ) on a Au crystal. Inset: measurement configuration schematic. (b) Critical current  $I_c^{A_i-B_i}$  versus temperature: experimental data (dots) and theoretical fits (lines) with interface transmission  $D = 0.03$ . (c) Model for Josephson current calculation in a single junction.

200mK)  $\approx I_c^{A_4-B_4}(T = 200\text{mK}) = I_c^o$ , which are also close to each other and are smaller than  $I_c^m$  by a factor of  $I_c^o/I_c^m \approx 7/8$ . This occurs despite the monotonic increase of  $L_i^{JJ}$  from  $A_1$ – $B_1$  to  $A_4$ – $B_4$ , indicating that the four JJs are not independent. Using the Au Fermi velocity  $v_F = 1.4 \times 10^6 \text{ m s}^{-1}$  and Al critical temperature  $T_c = 0.95 \text{ K}$ , the ballistic coherence length is  $\xi = v_F/2\pi T_c = 1.7 \mu\text{m}$ , exceeding all  $L_i^{JJ}$  and comparable to inter-electrode distances. Thus, Josephson coupling occurs between all superconducting lead pairs.

Existing theories for planar SN/N/NS structures assume either diffusive transport or purely ballistic trajectories, neither of which is applicable here. The Au crystal thickness  $d$  is less than the mean free path, and its width significantly exceeds the electrode dimensions. Moreover, no direct ballistic trajectories connect the leads; only trajectories involving reflections contribute [Fig. 1(b)]. Previous ballistic junction models [51, 52] assume translationally invariant infinite leads, which are inadequate for multiterminal structures. We develop a theoretical approach for strongly coupled planar Josephson structures on large crystals, detailed in a companion work [53]. Here, we apply it to our Al/Au/Al junctions.

If the thickness of the normal metal is large compared to the mean free path and the coherence length, that is  $d \gtrsim (\xi, l)$ , then the main contribution to the Josephson current is given by the impurity scattering in the normal layer. If the opposite case  $d \ll (\xi, l)$  occurs, the main contribution to the current is provided via the mechanism of reflections from the surfaces of the normal crystal. Our experiment corresponds to the second case, and

for this reason, we focus on this limit, while a more complete theory is discussed in the companion paper [53]. The calculation of the Josephson current is based on the Eilenberger equation for the quasiclassical Green's function  $\check{g}(\mathbf{n}, \mathbf{r}, \omega)$ , which is a matrix  $2 \times 2$  in the particle-hole space[54, 55]

$$[i\omega\tau_z + \begin{pmatrix} 0 & \Delta \\ -\Delta^* & 0 \end{pmatrix}, \check{g}] + iv_F \nabla \check{g} = 0, \quad (1)$$

where  $\omega$  is the fermionic Matsubara frequency,  $\Delta$  is the superconducting order parameter, which is nonzero only in the leads, and  $\tau_z$  is the Pauli matrix in the particle-hole space. We neglect the impurity scattering in the normal layer; for this reason, the impurity self-energy does not appear in Eq. (1). Assuming that the transmission  $D$  of the interface between superconductor and normal metal (S/N) is small,  $D \ll 1$ , as confirmed by subsequent comparisons of the calculated results with experimental data for the critical current amplitudes, the boundary conditions at the S/N interface take the form [56]:

$$\check{g}_N^{out} - \check{g}_N^{in} = \frac{D}{2} [\check{g}_N^0, \check{g}_S^0], \quad (2)$$

where  $\check{g}^{in(out)}$  is the Green's function incoming to (or outgoing from) the N side of the S/N interface, and  $\check{g}_{N(S)}^0$  is the Green's function in the normal metal (or superconductor) at  $D = 0$ . The complete system of equations required to calculate the Green's function in the normal layer and the Josephson current also contains boundary conditions at the upper and bottom surfaces of the N

layer. Depending on their roughness, the reflection process at these surfaces may contain both a specular and a diffusive component. For surface roughness, we consider specular reflection and isotropic diffusive scattering from the bottom N surface [Fig. 1(c)]. The diffusive scattering model agrees better with the experiment, suggesting relatively diffusive surfaces. The bottom surface boundary condition is:

$$\check{g}_N^{out} = \langle \check{g}_N^{in} \rangle, \quad (3)$$

where  $\langle \check{g}_N^{in} \rangle$  is the Green's function averaged over all the incoming directions of the electron velocity  $\mathbf{v}_F$ . The Josephson current between two arbitrarily small superconducting elements of the whole Josephson structure, presented in Fig. 1(a), takes the form [53]:

$$I_{S \rightarrow R} = T \sum_{\omega} \frac{D^2 e |\Delta|^2 dS_S dS_R N_F \lambda^2 v_F \sin(\phi_2 - \phi_1)}{8\pi(|\Delta|^2 + \omega^2)} \times \\ \int_0^{\pi} \int_{-\pi/2}^{\pi/2} \frac{e^{\tilde{d} - \sqrt{\tilde{d}^2 + \tilde{L}^2 - 2\tilde{L}\tilde{d}\cos\theta}\tilde{d}}}{(\tilde{d}^2 + \tilde{L}^2 - 2\tilde{L}\tilde{d})^{3/2}} \sin\theta d\theta d\varphi \quad (4)$$

where  $dS_{S,R}$  are areas of the corresponding superconducting elements,  $N_F$  is the electron density of states at the Fermi surface in the normal layer,  $|\Delta|$  is the absolute value of the superconducting order parameter, which is assumed to be the same in all superconducting leads,  $\phi_{1,2}$  are the phases of the superconducting order parameter of the considered elements,  $L$  is the distance between the elements, and  $\lambda = 2\omega/v_F$ .  $\tilde{L} = \lambda L$ ,  $\tilde{d} = \frac{\lambda d}{\cos\varphi\sin\theta}$ ,  $\theta$ , and  $\varphi$  are spherical angles of the scattering point in a coordinate system with the origin at one of the superconducting elements and the polar axis along the line connecting these elements. A good approximation is:

$$I_{S \rightarrow R} = T \sum_{\omega} \frac{D^2 e |\Delta|^2 dS_S dS_R N_F \lambda^2 v_F \sin(\phi_2 - \phi_1)}{8\pi(|\Delta|^2 + \omega^2)} \times \\ \frac{2}{\lambda^2(L^2 + 4d^2)} (2e^{-\lambda\sqrt{L^2 + 4d^2}} + e^{-\lambda(L+2d)}) \quad (5)$$

In this model, the multiple diffusive reflections from the N layer surfaces are disregarded. This approximation works well if  $\xi < d < l$  or  $L \lesssim 2d$ . The first of the conditions is not applicable to the current experiment, but the second condition is fulfilled for part of the JJs.

To calculate the net critical current  $I_c^{A_i - B_i}$  corresponding to the current flow from  $A_i$  to  $B_i$  electrodes, we first calculate the critical currents  $i_c^{A(B)_i - A(B)_j}$  between all possible pairs of  $A(B)_i - A(B)_j$  and  $A_i - B_j$  by summing the currents over all pairs of small superconducting elements belonging to the corresponding leads (28 JJs in total). Then the superconducting phases are set at two

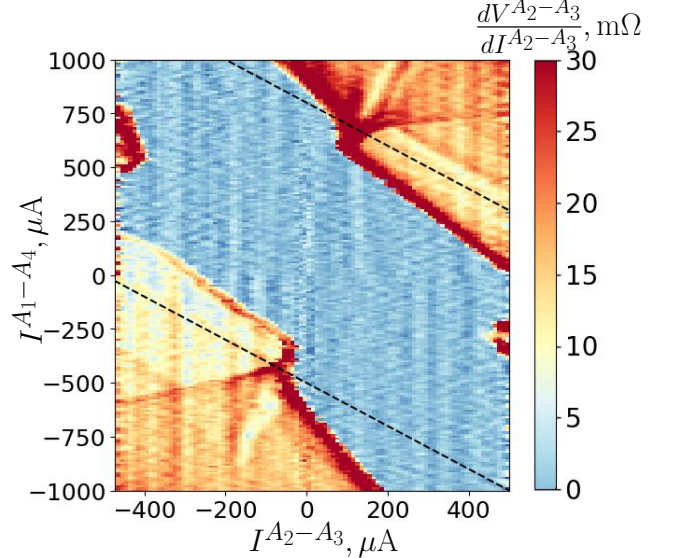


FIG. 2. Differential resistance  $dV/dI$  at the  $A_2 - A_3$  junction with simultaneous currents  $I^{A_2 - A_3}$  and  $I^{A_1 - A_4}$ .  $T = 0.7$  K.

leads through which the current is passed, and the other phases are determined numerically from the condition of current conservation [53].

In Fig. 1(b), the calculated  $I_c^{A_i - B_i}$  JJs for  $i = 1 - 4$  are superimposed on the experimental data. The model provides very good quantitative agreement for the low-temperature values of all four critical currents  $I_c^{A_i - B_i}$ . The overall nearly linear temperature dependence of the critical current is also reproduced, although the quantitative agreement between theory and experiment at intermediate temperatures is not ideal. In the experiment, the deviation of the  $I_c(T)$  from linearity occurs at lower temperatures than the theory suggests. In our opinion, this is due to the fact that, in the experiment, the interlayer lengths of most JJs are of the same order as the mean free path  $l$ ; therefore, the ballistic limit condition is not fully satisfied. That is, in addition to diffusive reflection from the surfaces of the N layer, there is also a certain amount of reflection from impurities in the N layer itself, which changes the temperature dependence of the coherence length.

*Multiterminal transport.*—Fig. 2 shows the resistance  $dV/dI$  measured at the  $A_2 - A_3$  JJ when the current  $I^{A_2 - A_3}$  is applied from  $A_2$  to  $A_3$  and the current  $I^{A_1 - A_4}$  is applied from  $A_1$  to  $A_4$  simultaneously. These data provide evidence of the multi-terminal behavior of our system, demonstrating that  $I^{A_2 - A_3}$  depends not only on the phase difference at the  $A_2 - A_3$  JJ but also on the phases at other superconducting electrodes. Indeed, if  $I^{A_i - A_j}$  is only determined by the phase difference at the  $A_i - A_j$  JJ between the nearest neighbor electrodes, then the system of  $A_1$ ,  $A_2$ ,  $A_3$ , and  $A_4$  electrodes on top of the Au crystal can be viewed as a chain of three JJs in

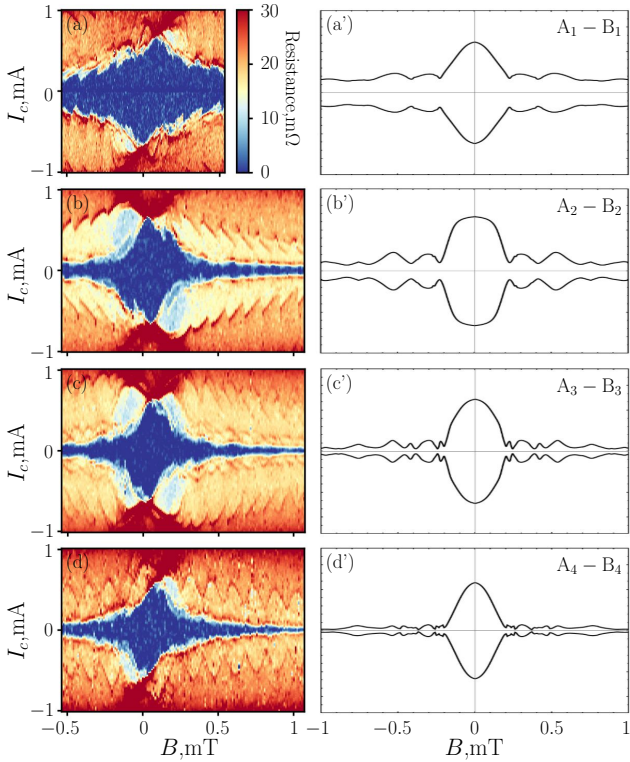


FIG. 3. (a)-(d) Experimental data for  $I_c^{A_i-B_i}$  (dark blue region boundaries) versus perpendicular magnetic field. (a')-(d') Theoretical results for  $I_c^{A_i-B_i}$  versus perpendicular magnetic field.  $T = 0.7$  K.

series:  $A_1 - A_2$ ,  $A_2 - A_3$ , and  $A_3 - A_4$ . In this case, the boundary of the blue region is determined by the condition  $I^{A_2-A_3} + I^{A_1-A_4} = \pm i_c^{A_2-A_3}$ . This means that the slopes of the blue region boundaries should be equal to -1 (shown as black dotted lines in Fig. 2), and the observed slopes are  $\approx -1.7$ . It indicates that, for example,  $I_c^{A_1-A_3} \neq 0$  and, therefore,  $I_c^{A_2-A_3}$  depend on the phases at all the electrodes.

*Magnetic field response.*—The experimental data for the dependence of  $I_c^{A_i-B_i}$  on the applied magnetic field  $B$  are presented in Figs. 3(a)-(d). First of all, one can see that the period of the Fraunhofer-like oscillations of  $I_c^{A_i-B_i}$  is approximately two orders of magnitude smaller than expected for an independent JJ  $B_p = \Phi_0/(L_i^{JJ}w)$ , where  $\Phi_0 = \pi\hbar c/e$  is the flux quantum.  $B_p = 3 \sim 30$  mT for  $i \in [1, \dots, 4]$ . The observed period approximately corresponds to the large area of the normal interlayers of the  $A(B)_i - A(B)_j$  JJs between the nearest neighbors  $i$  and  $j$ . It once again proves our main statement that, due to the quasi-ballistic regime of transport corresponding to the large coherence length  $\xi \approx 1.7\mu\text{m}$ , the Josephson coupling occurs between all the superconducting elements in the system. The asymmetry of positive and negative maxima of  $I_c$  can be explained by the magnetic self-fields of the Josephson currents, which are not taken into account in our theoretical consideration.

In order to calculate the dependence  $I_c(B)$ , the expressions for the critical current should be generalized in a standard way [57] by adding the integral of the magnetic field vector potential  $\mathbf{A}$  to the superconducting phase difference:

$$\phi_2 - \phi_1 \rightarrow \phi_2 - \phi_1 + \frac{2\pi}{\Phi_0} \int \mathbf{A}(s) \cdot \mathbf{n} ds \quad (6)$$

where  $\mathbf{n}$  is the unit vector along the trajectory and  $s$  is the coordinate along it. The results of the calculation [53] are presented in Figs. 3(a')-(d'). The theory reproduces well both the maximum current amplitude at  $B = 0$  and all the main features of the curves: a sharp drop in the critical current at a field of  $\sim 0.2$  mT, which is the same for all JJ, followed by a weakly decaying behavior on which quasi-periodic oscillations are superimposed. The initial sharp drop at  $B \sim 0.2$  mT is attributed to the first minimum of the Fraunhofer pattern of  $i_c^{A(B)_i - A(B)_j}$  and is located at  $B \approx \Phi_0/(L_i^{A(B)}W)$ . At larger fields, the main contribution to the current is produced by  $A_i - B_i$  JJs, which have a much smaller area of the normal interlayer region and a much weaker, non-oscillating dependence on the field [53]. It is important that at  $B > 0.2$  mT, when the contribution of the  $A(B)_i - A(B)_j$  JJs is strongly suppressed, the  $A_i - B_i$  JJs become practically independent. For this reason, the average critical current at  $B > 0.2$  mT, which corresponds to  $i_c^{A_i-B_i}$ , monotonically decreases with increasing  $L_i^{JJ}$  from  $i = 1$  to 4. The quasiperiodic character of the oscillations is the result of the superimposition of the Fraunhofer patterns corresponding to  $A(B)_i - A(B)_j$  JJs, which correspond to slightly different  $L_i^{A(B)}$ .

*Conclusions.*—We demonstrate a multi-terminal superconducting system on a Au single crystal in the quasi-ballistic regime, where the superconducting coherence length is comparable to inter-electrode distances. The nonmonotonic critical current dependence on interlayer length, distinctive magnetic field response showing a sharp regime crossover, and direct multiterminal transport measurements provide compelling evidence for strong coupling among all superconducting leads. Our results establish a platform for exploring multi-terminal Josephson effects, including artificial topological matter in metallic mesoscopic devices, where the entire Au crystal serves as the normal scattering region [53]. The developed theoretical approach for strongly coupled planar Josephson structures on large quasi-ballistic crystals agrees well with experiments, strongly supporting our interpretation.

We thank Sir A. Geim and E. Nguyen for the fruitful discussions. The experimental part of the work is supported by a grant from the Ministry of Science and Higher Education of the Russian Federation No 075-15-2025-010 from 28.02.2025.

---

[1] B. Josephson, Possible new effects in superconductive tunnelling, *Physics Letters* **1**, 251 (1962).

[2] T. Hoss, C. Strunk, T. Nussbaumer, R. Huber, U. Staufer, and C. Schönenberger, Multiple andreev reflection and giant excess noise in diffusive superconductor/normal-metal/superconductor junctions, *Physical Review B* **62**, 4079 (2000).

[3] M. Jung, H. Noh, Y.-J. Doh, W. Song, Y. Chong, M.-S. Choi, Y. Yoo, K. Seo, N. Kim, B.-C. Woo, B. Kim, and K. J., Superconducting junction of a single-crystalline au nanowire for an ideal josephson device, *Acs Nano* **5**, 2271 (2011).

[4] J. Wang, C. Shi, M. Tian, Q. Zhang, N. Kumar, J. Jain, T. Mallouk, and M. Chan, Proximity-induced superconductivity in nanowires: Minigap state and differential magnetoresistance oscillations, *Physical review letters* **102**, 247003 (2009).

[5] S. V. Sotничук, O. V. Skryabina, A. G. Shishkin, S. V. Bakurskiy, M. Y. Kupriyanov, V. S. Stolyarov, and K. S. Napol'skii, Long single au nanowires in nb/au/nb josephson junctions: Implications for superconducting microelectronics, *ACS Applied Nano Materials* **5**, 17059 (2022).

[6] R. B. van Dover, A. de Lozanne, and M. R. Beasley, Superconductor-normal-superconductor microbridges: Fabrication, electrical behavior, and modeling, *Journal of Applied Physics* **52**, 7327 (1981).

[7] H. Nakano and T. Aomine, Magnetic field dependence of critical currents in sns bridges fabricated by direction of sputtering deposition and anodic oxidization, *Japanese journal of applied physics* **26**, 304 (1987).

[8] H. Nakano and T. Aomine, Nb–cu–nb bridges fabricated by direction of sputtering deposition and anodic oxidization, *Japanese journal of applied physics* **25**, L601 (1986).

[9] H. Nakano and T. Aomine, Fabrication procedure of sns bridges by shapes of sputtering deposition at step edge and anodic oxidization, *Shinku* **30**, 188 (1987).

[10] F. Ichikawa, T. Fukami, and T. Aomine, Current-voltage characteristics of a triangular loop containing three sns bridges, *Physica C: Superconductivity* **221**, 195 (1994).

[11] P. Dubos, H. Courtois, B. Pannetier, F. Wilhelm, A. Zaikin, and G. Schön, Josephson critical current in a long mesoscopic sns junction, *Physical Review B* **63**, 064502 (2001).

[12] A. Savin, J. P. Pekola, J. Flyktman, A. Anthore, and F. Giazotto, Cold electron josephson transistor, *Applied physics letters* **84**, 4179 (2004).

[13] C. P. García and F. Giazotto, Josephson current in nanofabricated v/cu/v mesoscopic junctions, *Applied Physics Letters* **94**, 132508 (2009).

[14] T. E. Golikova, F. Hübner, D. Beckmann, N. V. Klenov, S. V. Bakurskiy, M. Y. Kupriyanov, I. Batov, and V. V. Ryazanov, Critical current in planar sns josephson junctions, *JETP letters* **96**, 668 (2013).

[15] T. Golikova, M. Wolf, D. Beckmann, I. Batov, I. Bobkova, A. Bobkov, and V. Ryazanov, Nonlocal supercurrent in mesoscopic multiterminal sns josephson junction in the low-temperature limit, *Physical Review B* **89**, 104507 (2014).

[16] M. Crosser, J. Huang, F. Pierre, P. Virtanen, T. T. Heikkilä, F. Wilhelm, and N. O. Birge, Nonequilibrium transport in mesoscopic multi-terminal sns josephson junctions, *Physical Review B—Condensed Matter and Materials Physics* **77**, 014528 (2008).

[17] L. Angers, F. Chiodi, G. Montambaux, M. Ferrier, S. Guéron, H. Bouchiat, and J. C. Cuevas, Proximity dc squids in the long-junction limit, *Phys. Rev. B* **77**, 165408 (2008).

[18] A. Morpurgo, T. Klapwijk, and B. Van Wees, Hot electron tunable supercurrent, *Applied physics letters* **72**, 966 (1998).

[19] Y. P. Baryshev, A. Vasil'ev, A. Dmitriyev, M. Y. Kupriyanov, V. Lukichev, I. Y. Luk'yanova, A. Orlikovskiy, and I. Sokolova, Theoretical and experimental study of the josephson effect in submicron sn-n-ns structures, *Lithography in microelectronics* **8**, 187 (1989).

[20] O. Skryabina, S. Bakurskiy, V. Ruzhickiy, A. Shishkin, N. Klenov, I. Soloviev, M. Y. Kupriyanov, and V. Stolyarov, Anomalous influence of electrode width on the critical current of nb/au josephson junctions, *Superconductor Science and Technology* **37**, 125018 (2024).

[21] A. A. Golubov, M. Y. Kupriyanov, and E. Il'ichev, The current-phase relation in josephson junctions, *Rev. Mod. Phys.* **76**, 411 (2004).

[22] I. Soloviev, S. Bakurskiy, V. Ruzhickiy, N. Klenov, M. Kupriyanov, A. Golubov, O. Skryabina, and V. Stolyarov, Miniaturization of josephson junctions for digital superconducting circuits, *Phys. Rev. Appl.* **16**, 044060 (2021).

[23] V. Ruzhickiy, S. Bakurskiy, M. Kupriyanov, N. Klenov, I. Soloviev, V. Stolyarov, and A. Golubov, Contribution of processes in sn electrodes to the transport properties of sn-n-ns josephson junctions, *Nanomaterials* **13**, 10.3390/nano13121873 (2023).

[24] V. Bosboom, J. van der Vegt, M. Yu Kupriyanov, and A. Golubov, Selfconsistent 3d model of sn-n-ns josephson junctions, *Superconductor science and technology* **34**, 10.1088/1361-6668/ac2d79 (2021), publisher Copyright: © 2021 The Author(s). Published by IOP Publishing Ltd.

[25] P. M. Marychev and D. Y. Vodolazov, A josephson junction based on a highly disordered superconductor/low-resistivity normal metal bilayer, *Beilstein Journal of Nanotechnology* **11**, 858 (2020).

[26] S. Bakurskiy, V. Ruzhickiy, A. Neilo, N. Klenov, I. Soloviev, A. Elistratova, A. Shishkin, V. Stolyarov, and M. Kupriyanov, text": "thouless energy in josephson sn-n-ns bridges, *Mesoscience & Nanotechnology* **1**, 10.64214/jmsn.01.01003 (2024).

[27] V. E. Calado, S. Goswami, G. Nanda, M. Diez, A. R. Akhmerov, K. Watanabe, T. Taniguchi, T. M. Klapwijk, and L. M. K. Vandersypen, Ballistic josephson junctions in edge-contacted graphene, *Nature Nanotechnology* **10**, 761 (2015).

[28] M. Ben Shalom, M. J. Zhu, V. I. Fal'ko, A. Mishchenko, A. V. Kretinin, K. S. Novoselov, C. R. Woods, K. Watanabe, T. Taniguchi, A. K. Geim, and J. R. Prance, Quantum oscillations of the critical current and high-field superconducting proximity in ballistic graphene, *Nature Physics* **12**, 318 (2016).

[29] M. T. Allen, O. Shtanko, I. C. Fulga, A. R. Akhmerov, K. Watanabe, T. Taniguchi, P. Jarillo-Herrero, L. S. Levitov, and A. Yacoby, Spatially resolved edge currents and guided-wave electronic states in graphene, *Nature Physics* **12**, 128 (2016).

[30] P. Kumaravadivel and X. Du, Signatures of evanescent transport in ballistic suspended graphene-superconductor junctions, *Scientific Reports* **6**, 24274 (2016).

[31] I. V. Borzenets, F. Amet, C. T. Ke, A. W. Draelos, M. T. Wei, A. Seredinski, K. Watanabe, T. Taniguchi, Y. Bomze, M. Yamamoto, S. Tarucha, and G. Finkelstein, Ballistic graphene josephson junctions from the short to the long junction regimes, *Phys. Rev. Lett.* **117**, 237002 (2016).

[32] M. Zhu, M. Ben Shalom, A. Mishchsenko, V. Fal'ko, K. Novoselov, and A. Geim, Supercurrent and multiple andreev reflections in micrometer-long ballistic graphene josephson junctions, *Nanoscale* **10**, 3020 (2018).

[33] B. van Heck, S. Mi, and A. R. Akhmerov, Single fermion manipulation via superconducting phase differences in multiterminal josephson junctions, *Phys. Rev. B* **90**, 155450 (2014).

[34] R.-P. Riwar, M. Houzet, J. S. Meyer, and Y. V. Nazarov, Multi-terminal josephson junctions as topological matter, *Nature Communications* **7**, 11167 (2016).

[35] L. Peralta Gavensky, G. Usaj, and C. A. Balseiro, Multi-terminal josephson junctions: A road to topological flux networks, *Europhysics Letters* **141**, 36001 (2023).

[36] A. H. Pfeffer, J. E. Duvauchelle, H. Courtois, R. Mélin, D. Feinberg, and F. Lefloch, Subgap structure in the conductance of a three-terminal josephson junction, *Phys. Rev. B* **90**, 075401 (2014).

[37] E. Strambini, S. D'Ambrosio, F. Vischi, F. S. Bergeret, Y. V. Nazarov, and F. Giazotto, The  $\omega$ -squipt as a tool to phase-engineer josephson topological materials, *Nature Nanotechnology* **11**, 1055 (2016).

[38] F. Vischi, M. Carrega, E. Strambini, S. D'Ambrosio, F. S. Bergeret, Y. V. Nazarov, and F. Giazotto, Coherent transport properties of a three-terminal hybrid superconducting interferometer, *Phys. Rev. B* **95**, 054504 (2017).

[39] Y. Cohen, Y. Ronen, J.-H. Kang, M. Heiblum, D. Feinberg, R. Mélin, and H. Shtrikman, Non-local supercurrent of quartets in a three-terminal josephson junction, *Proceedings of the National Academy of Sciences* **115**, 6991 (2018), <https://www.pnas.org/doi/pdf/10.1073/pnas.1800044115>.

[40] G. V. Graziano, J. S. Lee, M. Pendharkar, C. J. Palmstrøm, and V. S. Pribiag, Transport studies in a gate-tunable three-terminal josephson junction, *Phys. Rev. B* **101**, 054510 (2020).

[41] N. Pankratova, H. Lee, R. Kuzmin, K. Wickramasinghe, W. Mayer, J. Yuan, M. G. Vavilov, J. Shabani, and V. E. Manucharyan, Multiterminal josephson effect, *Phys. Rev. X* **10**, 031051 (2020).

[42] G. V. Graziano, M. Gupta, M. Pendharkar, J. T. Dong, C. P. Dempsey, C. Palmstrøm, and V. S. Pribiag, Selective control of conductance modes in multi-terminal josephson junctions, *Nature Communications* **13**, 5933 (2022).

[43] J. Kolzer, A. R. Jalil, D. Rosenbach, L. Arndt, G. Mussler, P. Schüffelgen, D. Grutzmacher, H. Luth, and T. Schapers, Supercurrent in  $\text{Bi}_4\text{Te}_3$  topological material-based three-terminal junctions, *Nanomaterials* **13**, 10.3390/nano13020293 (2023).

[44] A. W. Draelos, M.-T. Wei, A. Seredinski, H. Li, Y. Mehta, K. Watanabe, T. Taniguchi, I. V. Borzenets, F. Amet, and G. Finkelstein, Supercurrent flow in multi-terminal graphene josephson junctions, *Nano Letters* **19**, 1039 (2019).

[45] E. G. Arnault, T. F. Q. Larson, A. Seredinski, L. Zhao, S. Idris, A. McConnell, K. Watanabe, T. Taniguchi, I. Borzenets, F. Amet, and G. Finkelstein, Multiterminal inverse ac josephson effect, *Nano Letters* **21**, 9668 (2021).

[46] K.-F. Huang, Y. Ronen, R. Mélin, D. Feinberg, K. Watanabe, T. Taniguchi, and P. Kim, Evidence for  $4e$  charge of cooper quartets in a biased multi-terminal graphene-based josephson junction, *Nature Communications* **13**, 3032 (2022).

[47] M. Brust, M. Walker, D. Bethell, D. J. Schiffrin, and R. Whyman, Synthesis of thiol-derivatised gold nanoparticles in a two-phase liquid-liquid system, *Journal of the Chemical Society, Chemical Communications*, 801 (1994).

[48] B. Radha and G. Kulkarni, A real time microscopy study of the growth of giant au microplates, *Crystal growth & design* **11**, 320 (2011).

[49] S. G. Menabde, S. Boroviks, J. Ahn, J. T. Heiden, K. Watanabe, T. Taniguchi, T. Low, D. K. Hwang, N. A. Mortensen, and M. S. Jang, Near-field probing of image phonon-polaritons in hexagonal boron nitride on gold crystals, *Science advances* **8**, eabn0627 (2022).

[50] M. Onodera, Y. Wakafuji, T. Hashimoto, S. Masubuchi, R. Moriya, Y. Zhang, K. Watanabe, T. Taniguchi, and T. Machida, All-dry flip-over stacking of van der waals junctions of 2d materials using polyvinyl chloride, *Scientific Reports* **12**, 21963 (2022).

[51] M. Y. Kupriyanov, V. F. Lukichev, and A. A. Orlikovskii, Stationary properties of quasi-two-dimensional josephson weak links, *Microelectronics (in Russian)* **15**, 328 (1986).

[52] M. Y. Kupriyanov and V. F. Lukichev, Influence of proximity effect in electrodes and interface transparency on stationary properties of clean josephson sns structures, *Proceedings of the Institute of General Physics of RAS (in Russian)* **14**, 160 (1988).

[53] G. A. Bobkov, I. V. Bobkova, A. M. Bobkov, K. B. Polevoy, V. S. Stolyarov, and A. Geim, Theory of planar quasi-ballistic josephson junctions, (2025).

[54] G. Eilenberger, Transformation of gorkov's equation for type ii superconductors into transport-like equations, *Zeitschrift für Physik A Hadrons and nuclei* **214**, 195 (1968).

[55] A. Larkin and Y. N. Ovchinnikov, Quasi-classical method in the theory of superconductivity, *Zh. Eksp. Teor. Fiz.* **55** (1968), [Sov. Phys. JETP **28**, 1200 (1969)].

[56] A. V. Zaitsev, Quasiclassical equations of the theory of superconductivity for contiguous metals and the properties of constricted microcontacts, *Sov. Phys. JETP* **59** (1984).

[57] V. Barzykin and A. M. Zagoskin, Coherent transport and nonlocality in mesoscopic sns junctions: anomalous magnetic interference patterns, *Superlattices and Microstructures* **25**, 797 (1999).